






Polarized light emission from graphene induced by terahertz pulsesI. V. Oladyshkin ^{*}, S. B. Bodrov , A. V. Korzhimanov , A. A. Murzanev, Yu. A. Sergeev , A. I. Korytin ,
M. D. Tokman, and A. N. Stepanov*Institute of Applied Physics of the Russian Academy of Sciences, 603950 Nizhny Novgorod, Russia*

(Received 8 April 2022; revised 13 September 2022; accepted 26 October 2022; published 10 November 2022)

Spontaneous optical emission of graphene irradiated by intense single-cycle terahertz pulses was studied experimentally and explained theoretically. We found that the emitted photons are mainly polarized normally to the electric field of the terahertz pulse, which proves that the terahertz field not only heats the electrons, but also creates a strongly nonequilibrium momentum distribution. The comparison of the measured optical spectrum and polarization anisotropy with the results of numerical modeling allowed us to estimate the momentum isotropization time for electrons in graphene to be ~ 25 fs and roughly reconstruct the time evolution of the distribution function in k space.

DOI: [10.1103/PhysRevB.106.205407](https://doi.org/10.1103/PhysRevB.106.205407)**I. INTRODUCTION**

Graphene is one of the promising materials attracting attention due to unusual properties of charge carriers and unique characteristics, such as two-dimensional (2D) geometry, high nonlinearity, record electrical and thermal conductivity, and others. Nonlinear and quantum optics of graphene has been actively investigated [1–14]. Over the past few years, ultrafast kinetics of the electrons in graphene became one of the central topics in a large number of fundamental and applied studies of various subpicosecond processes. In particular, it was found that femto- and picosecond relaxation processes play a key role in many effects, including nonlinear terahertz response [7,8,15], surface plasmon generation [10,11,16,17], nonlinear transmission [8,12], high harmonic generation [18–24], inverse Faraday effect, the generation of edge photocurrents [9,25], etc.

At the same time, the dynamics of elementary relaxation processes on ultrashort timescales in graphene and other materials is still a relevant problem due to limitations of available experimental techniques and high complexity of first-principles modeling. Worthy of mention is the recent attempt to control and measure the e - e electron scattering length in graphene in the experiment performed by Polini and collaborators [26]. Various pump-probe experiments (terahertz pump–optical probe [27], optical pump–terahertz probe [28], optical pump–optical probe [29–31]) and theoretical works [32–36] were devoted to the investigation of ultrafast carrier dynamics in graphene, especially the thermalization and recombination processes. In particular, it was demonstrated that the characteristic time of interband recombination (~ 1 ps) significantly exceeds the times of intraband carrier thermalization and cooling (100–300 fs) [12,27].

Terahertz-field-induced spontaneous optical emission in the 350–600 nm range was observed from monolayer

graphene on a glass substrate (at peak terahertz electric fields from 100 to 250 kV/cm) in Ref. [37]. To explain the experimental results an analytical theory based on electron-hole pair production by Schwinger-like (or Landau-Zener) transitions in a strong electric field was proposed. The thermal mechanism which can also contribute to the optical emission was estimated to be two orders weaker than the measured one. At the same time, in Ref. [27] the dominant role of impact ionization, or interband reverse Auger recombination, in the process of electron-hole pair production by strong terahertz field was stated¹.

In this paper we provide clearer experimental evidences of a strongly nonthermal character of terahertz-field-induced optical emission from graphene. For this we measured spectral and polarization properties of the optical emission in the spectral range of 350–1050 nm. In combination with the numerical modeling, this allowed us to prove the distribution function in k space to be significantly anisotropic and to estimate the collision frequency and the temperature of excited electrons.

¹In ideal 2D Dirac systems, interband reverse Auger recombination (impact ionization) is allowed only for electrons having collinear momenta due to the energy and momentum conservation laws [30,38,39]. Nevertheless, Auger processes play an important role in the thermalization of electrons, especially in weakly excited graphene. In a general case the efficiency of interband Auger processes is determined by the distortion of conservation laws: by the lattice imperfection (e.g., trigonal warping [40]), two-particle collisions in the presence of additional interaction with phonons [30,39], or others. This means that one should use fitting parameters in corresponding theory (see, e.g., Ref. [27]). As for the charge-carrier multiplication in the terahertz field, the theory based on Landau-Zener transitions (ballistic ionization) allowed us to explain experimental results without such heuristic assumptions [37]. Hence, we conclude that the role of Landau-Zener transitions in charge-carrier multiplication is dominant at strong excitation fields.

*oladyshkin@ipfran.ru

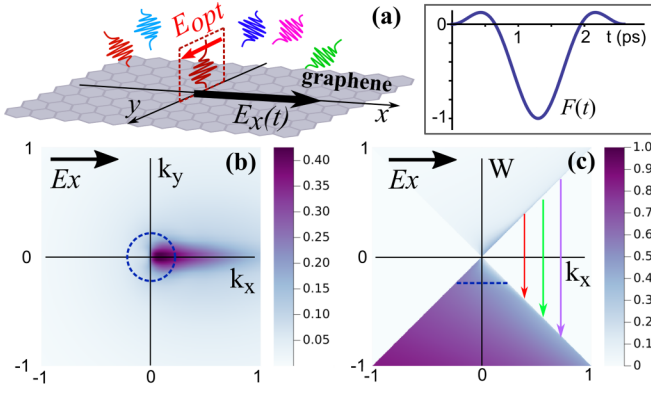


FIG. 1. (a) Geometry of the problem: terahertz electric field $E_{(x,t)} = E_{\text{THz}}F(t)$ oriented along the x axis induces spontaneous optical photons of different wavelengths with dominant polarization of electric field E_{opt} along the y axis. Inset: normalized waveform of the terahertz pulse $F(t)$ used in numerical modeling. (b) Numerically calculated distribution of electrons in k space of the conduction band at the moment of peak terahertz field ($E_{\text{THz}} = 190 \text{ kV/cm}$); the dashed blue circle depicts the initial Fermi level in the valence band. (c) The same distribution in energy space; the initial Fermi level is shown by the dashed blue line; possible direct interband transitions are shown by color arrows. In (b) and (c) color bars represent occupation probability and the unit scales of vertical and horizontal axes correspond to $W = 1 \text{ eV}$ and $\hbar k_{x,y} v_F = 1 \text{ eV}$.

II. THEORETICAL MODEL

Let us start with a theoretical model. Schematically, the optical emission from graphene induced by a strong terahertz field can be represented as a four-step process (Fig. 1):

(1) strong electron acceleration by the electric field of the terahertz pulse, $E_x(t) = E_{\text{THz}} \cdot F(t)$, where E_{THz} and $F(t)$ are the peak value and the normalized waveform of the terahertz field, respectively;

(2) electron-pair production by Schwinger-like (or Landau-Zener) transitions, leading to nonequilibrium electron distribution in k space;

(3) intraband isotropization of electron momenta (independently in the conduction and valence bands); and

(4) spontaneous interband electron-hole recombination accompanied by optical photon emission.

In our initial study [37] the intraband isotropization was assumed to be instantaneous. Here we do not use this assumption; instead, we model dynamics of the electronic distribution function in k space, including both isotropization and recombination. We use the density matrix equations for a two-band system in a homogeneous electric field [23], which is a version of the semiconductor Bloch equations:

$$\left(\frac{\partial}{\partial t} + i\omega_k + \gamma_a - \frac{eE_x(t)}{\hbar} \frac{\partial}{\partial k_x} \right) \rho_k = -i \frac{\Omega_k}{2} [n_c(\mathbf{k}) - n_v(\mathbf{k})], \quad (1)$$

$$\frac{\partial n_{c,v}(\mathbf{k})}{\partial t} - \frac{e}{\hbar} E_x(t) \frac{\partial n_{c,v}(\mathbf{k})}{\partial k_x} = \mp i \Omega_k \text{Im}(\rho_k) + R_{c,v}(\mathbf{k}), \quad (2)$$

where e is the elementary charge, \mathbf{k} is the electron wave vector, $n_{c,v}(\mathbf{k})$ are the electron populations in the conduction

and valence bands, respectively, i.e., the diagonal terms of 2×2 density matrix, $\rho_k = \rho_{cv;k\mathbf{k}}$ is the interband quantum coherence (off-diagonal terms), $\omega_k = 2v_F k$ is the local interband transition frequency at a given point of the k space, v_F is the Fermi velocity ($\sim 10^8 \text{ cm/s}$), $\Omega_k = \frac{e}{\hbar} \sin\theta_k E_x$ is the local Rabi frequency, θ_k is the angle between \mathbf{k} and the x axis, γ_a^{-1} is the relaxation time for the interband quantum coherence, and $R_{c,v}(\mathbf{k})$ are the phenomenological operators of the population relaxation in the conduction and valence bands, respectively.

The operators of population relaxation are set in the simplest form (Bhatnagar-Gross-Krook) with two characteristic timescales: “fast” intraband relaxation and “slow” interband recombination (described by γ_r):

$$R_{c,v}(\mathbf{k}) = -\gamma_a [n_{c,v}(\mathbf{k}) - n_{c,v}^F(k)] - \gamma_r [n_{c,v}(\mathbf{k}) - n_{0(c,v)}^F(k)]. \quad (3)$$

The intraband relaxation constant is supposed to be equal to the coherence relaxation rate γ_a . Here

$$n_{0(c,v)}^F(k) = \frac{1}{1 + \exp[(\pm v_F \hbar k / 2 - \mu_0) / T]} \quad (4)$$

is a globally equilibrium Fermi distribution with the initial chemical potential μ_0 , and

$$n_{c,v}^F(k) = \frac{1}{1 + \exp[(\pm v_F \hbar k / 2 - \mu_{c,v}) / T]} \quad (5)$$

are the quasiequilibrium local Fermi distributions in the conduction (c) and valence (v) bands, respectively, having a preset temperature of electrons T and time-dependent chemical potentials $\mu_{c,v}$. The chemical potentials $\mu_{c,v}$ are calculated independently using the normalization relations which include the charge-carrier density in each band at the current moment of time:

$$\iint_{\infty} n_c(\mathbf{k}) d^2k = 2\pi \int_0^{\infty} n_c^F(k) k dk, \\ \iint_{\infty} [1 - n_v(\mathbf{k})] d^2k = 2\pi \int_0^{\infty} [1 - n_v^F(k)] k dk. \quad (6)$$

It should be emphasized that the relaxation coefficients $\gamma_{a,r}$ for a single electron do not depend on its momentum k . At the same time, the relaxation rate of the total electron distribution is determined not only by these coefficients, but also by the local population difference [see the right-hand side of Eqs. (1) and (3)], which follows from the Pauli exclusion principle. This means that the relaxation time of the total electric current significantly depends on the specific shape of the electronic distribution function.

The discussed phenomenological model of relaxation might, in principle, include two different characteristic timescales of intraband relaxation: the isotropization time γ_{a1}^{-1} and the thermalization time γ_{a2}^{-1} instead of the universal constant γ_a^{-1} . Moreover, due to Auger processes, electron thermalization along a given direction of \mathbf{k} could be much faster than the isotropization at low excitation fluences and low pumping photon energies [12]. However, the case of intense terahertz field action differs significantly since the electronic distribution function occurs to be strongly perturbed and more spread out over the momentum space [see

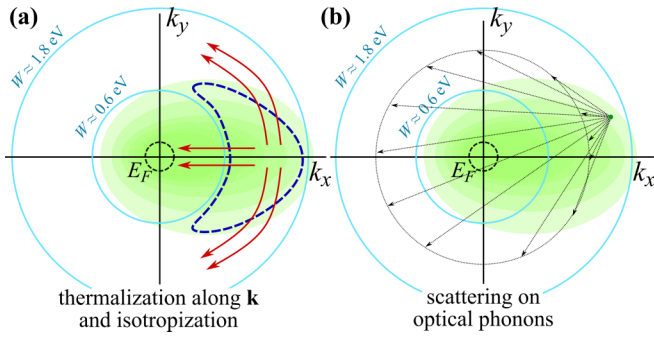


FIG. 2. Schematic picture of the electron scattering in k space of graphene excited by a strong terahertz pulse; the population probability is shown by green gradients. Solid blue circles show the electron energies corresponding to the boundaries of the measured photon spectrum (≈ 1.2 – 3.6 eV), so that only the interband transitions of electrons inside this ring are registered due to photon emission; the small dashed circle shows the initial Fermi level and the arrows show schematically possible directions of electron scattering. (a) Possible contribution of collinear (along \mathbf{k}) and azimuthal scattering to the decrease of the distribution anisotropy inside the circle. (b) Possible directions of electron scattering on optical phonons.

Figs. 1(b) and 2]. Because of that, many electronic states become “open” for both electron-electron and electron-phonon scattering. In particular, probability of the electron scattering on optical phonons increases dramatically compared to the case of weak excitation [see Fig. 2(b)], which should greatly accelerate the isotropization.

As shown in Fig. 2(a), both processes of electron thermalization along a given \mathbf{k} direction and distribution isotropization should contribute to the decrease of electron distribution anisotropy inside the measured region. Since we cannot *a priori* separate the contributions of these two processes, we introduced only one intraband relaxation parameter.

Based on the previously reported results, we suppose that under our experimental conditions we operate slightly below the region of temperature saturation caused by the strong heat absorption by optical phonons with the excitation energy of about 0.2 eV [37,41,42]. Hence, taking the electron temperature dependence on the peak terahertz field into consideration is essential for the development of a numerical model. For simplicity we assume the linear dependence $T(E_{\text{THz}})$. As for the interband recombination rate, the variation of γ_r^{-1} within a reasonable range of 0.3–1 ps does not significantly affect the distribution function shape obtained in simulations; so, we set it to be equal to 500 fs. The intraband relaxation time γ_a^{-1} , in contrast, significantly alters the polarization properties of the spontaneous emission, which allows us to estimate the anisotropy relaxation rate from experimental data.

The numbers of photons with x and y polarizations, spontaneously emitted due to the interband transitions, are calculated using the analytical relations given in the Appendix of Ref. [37], where the probability of spontaneous emission of photons with x and y polarization in the graphene with an arbitrary electron distribution $n_{c,v}(\mathbf{k})$ is found in a general form. In particular, in Ref. [37] it was shown that the interband transition of an electron moving along the x axis most probably leads to the generation of a photon polarized along the y

axis, and vice versa. To compare numerical simulations with the experimental results we found the total number of photons emitted during the terahertz pulse action (in the frequency range determined by the characteristics of the used optical filters). We also point out that at room temperature the interband relaxation is caused primarily by the electron-phonon interaction, so spontaneous emission of photons is a process with a relatively low probability, so it modifies the distribution function insignificantly.

The density matrix equations were discretized on a 2D rectangular grid and numerically integrated by an operator splitting method [43] as follows. The advection term $\partial/\partial t - eE/\hbar\partial/\partial k_{x,y}$ was integrated by means of the positivity flux conservative scheme [44] from the Vasilek.jl project [45]. Rabi terms and damping terms were calculated by a simple Euler scheme. A written code was tested against a number of simple problems with known results and was shown to be stable and reasonably accurate. A 300×100 box corresponding to the physical dimensions $[-1.5, 1.5] \times [-1.5, 1.5]$ measured in $\text{eV}/\hbar v_F$ was used in all simulations. The time step was $0.4 \text{ eV}^{-1} \hbar \approx 1.6 \text{ fs}$ and the total simulation time was 7000 time steps or about 11.6 ps. Initially the Fermi distribution was set with a given Fermi energy of -0.35 eV for a polyethylene terephthalate (PET) substrate and -0.2 eV for a glass substrate. Other parameters were varied as indicated in the text below.

A typical calculated distribution function of electrons in a strong terahertz field is shown in Figs. 1(b) and 1(c). The region of significant population perturbation extends up to the energy level of 0.5–1.0 eV, which corresponds to direct interband transitions with 1–2 eV energy. The calculations predict an intense electron-hole pair production with the density $N_c \cong 2.5 \times 10^{12} \text{ cm}^{-2}$ and significant anisotropy of the electron momenta. This density can also be calculated analytically in the ballistic ionization model ² [37]:

$$\frac{dN_c}{dt} = \left(\frac{eE_x}{\hbar} \right)^{3/2} \frac{(\bar{n}_v - \bar{n}_c)}{\pi^2 \sqrt{v_F}}, \quad (7)$$

where $\bar{n}_{v,c}$ are the averaged populations in the valence and conduction bands, respectively. Below we discuss the results of time-integrated measurements, so further estimations based on Eq. (7) contain the characteristic duration of the terahertz pulse τ_{THz} . Equation (7) predicts $N_c \cong 5 \times 10^{12} \text{ cm}^{-2}$ for the parameters like those used in Fig. 1, which overestimates the density obtained in the numerical modeling because Eq. (7) does not take into account the interband recombination.

The distribution function anisotropy can also be estimated analytically in the simplest model of relaxation. For this we introduce the parameter describing relative deformation of the distribution function $\eta = \delta k_x/k_F$, where $k_F = \sqrt{\pi N_c}$ is the “local” Fermi wave number in the conduction band and δk_x is the stationary shift of the distribution function in k space. In

²Equation (7) is valid when the time of the Landau-Zener transition $\delta t = \sqrt{\hbar/eE_x v_F}$ is less than the momentum relaxation time γ_a^{-1} [37]. Typically, this condition is fulfilled for terahertz fields stronger than 70–100 kV/cm ($\delta t = 8$ –10 fs), which is also the threshold of intense pair production.

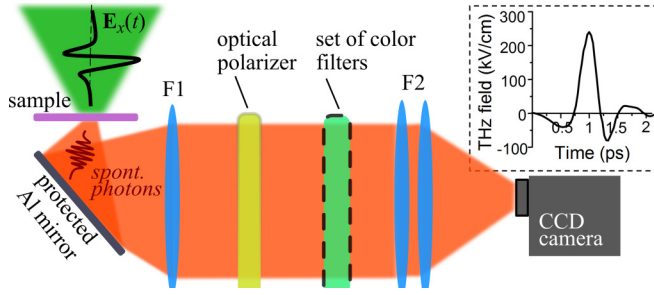


FIG. 3. Experimental setup. Inset: waveform of the terahertz pulse measured by time-domain spectroscopy.

the Drude model δk_x can be calculated as

$$\delta k_x = \frac{eE_x}{\hbar\gamma_a}. \quad (8)$$

Assuming that initially $\bar{n}_v \approx 1$, $\bar{n}_c \ll 1$ from Eq. (7) we obtain

$$\eta = \frac{\pi}{\gamma_a} \left(\frac{eE_{\text{THz}}v_F}{\hbar\tau_{\text{THz}}^2} \right)^{1/4}. \quad (9)$$

Thus, the relative deformation of the distribution function is proportional to $E_{\text{THz}}^{1/4}$, so the dependence is rather weak. This is a consequence of the competition between two physical effects: the growth of the local Fermi level in the conduction band [due to the increase of the electron density according to Eq. (7)] and the increase of the distribution function shift [according to Eq. (8)]. At the same time, the deformation parameter η determines the ratio between the number of spontaneous photons with y and x polarizations, which follows from the expressions for the probability of spontaneous emission of an electron with given momentum direction (see Appendix in Ref. [37]). Certainly, Eq. (9) is just an approximate relation suitable mostly for qualitative analysis of the polarization anisotropy dependence on the terahertz field. However, notice that the effect of the electron temperature growth with the increase of terahertz intensity will make this theoretical dependence even more flat, and so closer to the experimental one (see the more detailed comparison below).

III. EXPERIMENTAL RESULTS AND DISCUSSION

The experimental setup used for investigating the polarization and spectral properties of terahertz-field-induced luminescence of graphene is shown in Fig. 3 and is described in more detail in [37,46]. The single-cycle terahertz pulses generated by the tilted-pulse-front technique in a LiNbO_3 crystal were sharply focused on a graphene sample. The terahertz electric field was vertically polarized (along the x axis) and had a peak magnitude of up to ~ 250 kV/cm.

The optical luminescence emitted in the forward direction was collected by lens F1 ($D = 45$ mm and $\text{NA} = 0.8$) and focused by objective lens F2 (Canon EF 50 mm F/1.4) on a cooled CCD camera (SPEC-10:400BR, Princeton Instruments). Camera exposure was set to 100 s. A wide polarizer (25×25 mm; Thorlabs WP25L-UB) and a set of calibrated color filters were placed after lens F1 to measure the polarization and spectral properties of the luminescence. The number

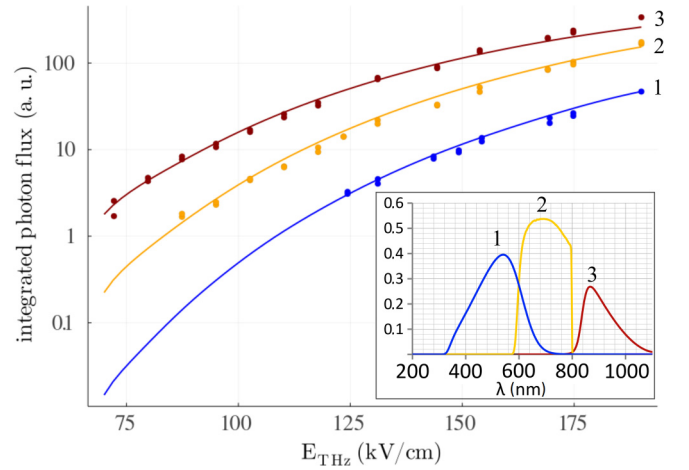


FIG. 4. Number of terahertz-field-induced optical photons in different spectral ranges as a function of peak terahertz field for the graphene on PET substrate. Experimental data and numerical calculations are shown by circles and color lines, respectively. Spectral characteristics of the used color filters (taking into account CCD camera spectral response) are given in the inset; the experimental points for the photon flux are plotted after normalization to the integral transitivity of the corresponding filter. The maximal absolute number of detected photons for filter No. 3 is about 1×10^6 per 6×10^4 shots at 190 kV/cm.

of emitted photons was calculated as a sum of CCD counts over the illuminated region (typically covering 50×50 pixels) with account of transparency of the corresponding color filters and spectral response of the detection system calibrated with a blackbody source (LS-1-LL) with a temperature of 2800 K.

We used two samples of chemical vapor deposition grown monolayer graphene: on a PET substrate (Graphenea, Inc.) and on a glass substrate (Graphene Supermarket). Note that the graphene doping was of the p type in both cases and the characteristic Fermi levels were -0.2 eV for glass and -0.35 eV for PET [47] substrates. Due to Fresnel reflection, the terahertz electric field in graphene was reduced by a factor of 1.25 and 1.67 for PET and glass substrates, respectively.

The number of emitted photons N_{ph} as a function of the peak terahertz electric field E_{THz} in three selected spectral ranges, 400–600, 600–850, and 850–1100 nm, is shown in Fig. 4 (the shorter the wavelength, the faster the gradient). Similarly to the previous results [37,46], the luminescence in each spectral range increased rapidly with the field strength. From the numerical calculations we found that $N_{\text{ph}}(E_{\text{THz}})$ was highly sensitive to temperature T . Satisfactory coincidence with the experiment was obtained for a linear fitting of the phenomenological dependence $T(E_{\text{THz}})$ introduced in the theoretical model:

$$T(E_{\text{THz}}) = 44 [\text{meV}] + 1.1 [\text{meV cm/kV}] \times E_{\text{THz}} [\text{kV/cm}]. \quad (10)$$

Of course, this linear dependence should be treated just as a local approximation valid in the studied range of electric fields; to propose more precise fittings, more experimental

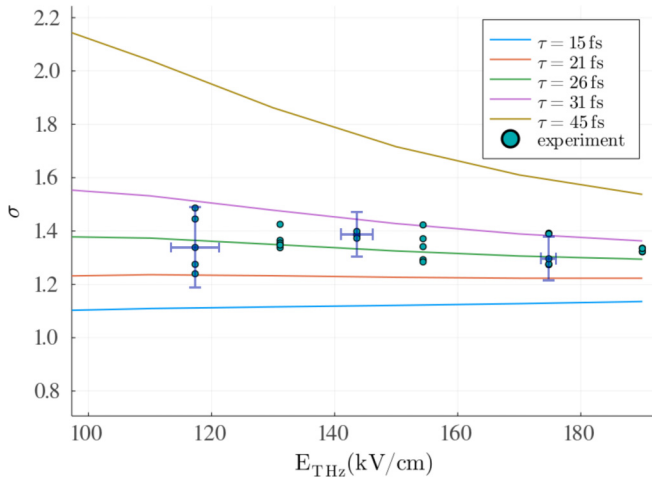


FIG. 5. Polarization anisotropy σ as a function of peak terahertz-field magnitude (photons were detected in the 350–1050 nm range). Circles, experimental data; color lines, numerical modeling results for different relaxation times γ_a^{-1} specified in the inset. Error bars are shown by blue crosses.

data in the $E_{\text{THz}} \leq 100 \text{ kV/cm}$ region are needed (other approximation functions with the same local slope give no significant difference for the available data interpretation). However, the presence of the $T(E_{\text{THz}})$ dependence in itself is of principal importance. This result does not contradict the previous estimates of electronic temperature in terahertz-excited graphene from Ref. [37], where no clear dependence was found in the range of the incident field of 200–300 kV/cm. In the paper [37] a two times narrower spectrum range was used, which limited the accuracy of temperature determination (at the same time, at a maximal incident terahertz field of 250 kV/cm, in this work we still obtain $T \approx 0.25 \text{ eV}$, as was measured in Ref. [37]).

From the experiment we found that the polarization anisotropy parameter σ , which is a ratio of the number of photons detected after the horizontal and vertical polarizers, remained roughly constant at $\sigma \approx 1.35$ in the available range of terahertz field magnitudes of 120–190 kV/cm (see Fig. 5). Notice that the scatter of the experimental points at a given terahertz-field magnitude is determined mostly by the long-term instability of the terahertz source (the main contribution to the experimental error), along with random fluctuations of the photon number at low excitation fields.

Numerical modeling showed that the function $\sigma(E_{\text{THz}})$ was modified significantly with the change of anisotropy relaxation time γ_a^{-1} . In particular, at $\gamma_a^{-1} = 45 \text{ fs}$ the polarization ratio decreased from 2.1 to 1.5 with the terahertz-field increase from 120 to 190 kV/cm, while at $\gamma_a^{-1} = 15 \text{ fs}$, in contrast, this dependence slightly increased near $\sigma \approx 1.1$. The best coincidence with the experimental data (the absolute value and the near-zero slope) was achieved for $\gamma_a^{-1} = 26 \pm 5 \text{ fs}$. Notice that the variations of both the interband relaxation rate γ_r and the electronic temperature within the experimental accuracy do not significantly affect the behavior of $\sigma(E_{\text{THz}})$.

The experimental results qualitatively agreed with the analytical Eq. (9), predicting the slowly growing dependence

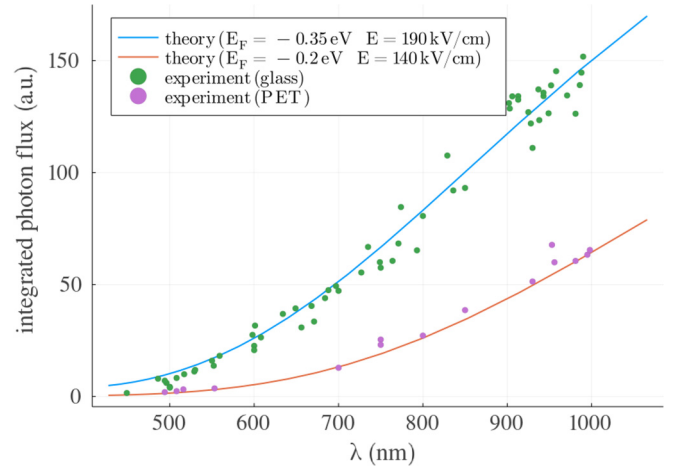


FIG. 6. Terahertz-field-induced luminescence spectra from graphene on PET (green points and blue curve) and glass (violet points and red curve) substrates. Experimental data, points; numerical modeling, curves. Initial Fermi levels and magnitude of the terahertz-field E_{THz} used in numerical modeling are given in the inset.

$\sigma(E_{\text{THz}})$ and giving the deformation parameter $\eta \cong 1.5$ for $\tau_{\text{THz}} = 200 \text{ fs}$ (see the inset in Fig. 3) and $\gamma_a^{-1} = 26 \text{ fs}$, which corresponds well to the measured σ . We emphasize that, although the characteristic time of terahertz-field variation ($\omega^{-1} \approx 150 \text{ fs}$) was larger than the intraband relaxation (20–30 fs), the resulting quasiequilibrium shift of the electronic distribution function in k space determined the emission polarization properties, which allowed us to draw the conclusions about the relaxation rate.

The optical emission spectra from graphene on the PET and glass substrates (measured for the incident terahertz field of 250 kV/cm) are shown in Fig. 6. For the sample with PET substrate the emission is about two times more intensive than for the sample with glass substrate. This is a result of different terahertz pulse magnitudes in graphene on PET and glass substrates (190 and 140 kV/cm, respectively) which gives, according to Eq. (10), different effective electron temperatures (0.25 and 0.2 eV, respectively). Numerical calculations for these samples without adjustable parameters, give emission spectra which agree well with the experiment both in the shape and in the magnitude (Fig. 6). This fact corroborates the proposed numerical model.

To conclude, we have investigated spontaneous optical emission of graphene with strongly nonequilibrium charge-carrier distribution excited by a single-cycle terahertz pulse. This broadband optical radiation has a quasithermal spectrum (in the range of 350–1050 nm) but is significantly polarized with prevailing polarization normally to the incident terahertz field. The polarization ratio was found to be approximately constant (about 1.35) for the terahertz-field magnitudes from 120 to 190 kV/cm. We interpreted these facts as a consequence of strong deformation of the electronic distribution function in graphene, which remains almost constant due to the competition between the field acceleration, scattering, and temperature growth processes.

The comparison of the experimental data with the numerical calculations allowed us to find the intraband relaxation

time 26 ± 5 fs and to reconstruct approximate electronic temperature dependence on terahertz field. The best fitting in the studied range of electric fields was achieved for $(E_{\text{THz}}) = 44$ [meV] + 1.1 [meV cm/kV] $\times E_{\text{THz}}$ [kV/cm], which can be used for further validation of microscopic heating models.

Finally, we emphasize that the observation of spontaneous optical emission after subpicosecond terahertz excitation is a powerful experimental method for obtaining new data on the ultrafast kinetics of nonequilibrium electrons in graphene, as well as in other materials. Being polarization sensitive by its nature, this method gives a possibility to study an ultrafast isotropization stage of the distribution function evolution.

ACKNOWLEDGMENTS

The experimental part of the work was financed by the RFBR (Grant No. 18-29-19091_mk); the operation of the laser system was supported by the Ministry of Science and Higher Education of the Russian Federation, state assignment for the Institute of Applied Physics RAS, Project No. 0030-2021-0012. Personally, I.V.O. thanks the Russian Science Foundation which supported the theoretical analysis and data interpretation (Project No.21-72-00076). The numerical simulations were performed on the resources provided by the Joint Supercomputer Center of the Russian Academy of Sciences. The authors also thank Alexey Belyanin for fruitful discussions.

-
- [1] F. Bonaccorso, Z. Sun, T. Hasan, and A. Ferrari, Graphene photonics and optoelectronics, *Nat. Photonics* **4**, 611 (2010).
- [2] T. Gu, N. Petrone, J. F. McMillan, A. van der Zande, M. Yu, G.-Q. Lo, D.-L. Kwong, J. Hone, and C. W. Wong, Regenerative oscillation and four-wave mixing in graphene optoelectronics, *Nat. Photonics* **6**, 554 (2012).
- [3] D. Sun, C. Divin, J. Rioux, J. E. Sipe, C. Berger, W. A. de Heer, P. N. First, and T. B. Norris, Coherent control of ballistic photocurrents in multilayer epitaxial graphene using quantum interference, *Nano Lett.* **10**, 1293 (2010).
- [4] Y. Q. An, F. Nelson, J. U. Lee, and A. C. Diebold, Enhanced optical second-harmonic generation from the current-biased graphene/SiO₂/Si(001) structure, *Nano Lett.* **13**, 2104 (2013).
- [5] H. K. Avetissian, A. K. Avetissian, G. F. Mkrtchian, and K. V. Sedrakian, Multiphoton resonant excitation of Fermi-Dirac sea in graphene at the interaction with strong laser fields, *J. Nanophotonics* **6**, 061702 (2012).
- [6] T. Jiang, V. Kravtsov, M. Tokman, A. Belyanin, and M. B. Raschke, Ultrafast coherent nonlinear nanooptics and nanoimaging of graphene, *Nat. Nanotechnol.* **14**, 838 (2019).
- [7] H. A. Hafez, S. Kovalev, K. J. Tielrooij, M. Bonn, M. Gensch, and D. Turchinovich, Terahertz nonlinear optics of graphene: From saturable absorption to high-harmonics generation, *Adv. Opt. Mater.* **8**, 1900771 (2020).
- [8] H. A. Hafez, S. Kovalev, J. C. Deinert *et al.*, Extremely efficient terahertz high-harmonic generation in graphene by hot Dirac fermions, *Nature (London)* **561**, 507 (2018).
- [9] M. Glazov and S. Ganichev, High frequency electric field induced nonlinear effects in graphene, *Phys. Rep.* **535**, 101 (2014).
- [10] X. Yao, M. Tokman, and A. Belyanin, Efficient Nonlinear Generation of THz Plasmons in Graphene and Topological Insulators, *Phys. Rev. Lett.* **112**, 055501 (2014).
- [11] T. J. Constant, S. M. Hornett, D. E. Chang, and E. Hendry, All-optical generation of surface plasmons in graphene, *Nat. Phys.* **12**, 124 (2016).
- [12] J. C. König-Otto, M. Mittendorff, T. Winzer, F. Kadi, E. Malic, A. Knorr, C. Berger, W. A. de Heer, A. Pashkin, H. Schneider, M. Helm, and S. Winnerl, Slow Noncollinear Coulomb Scattering in the Vicinity of the Dirac Point in Graphene, *Phys. Rev. Lett.* **117**, 087401 (2016).
- [13] T. Li, L. Luo, M. Hupalo, J. Zhang, M. C. Tringides, J. Schmalian, and J. Wang, Femtosecond Population Inversion and Stimulated Emission of Dense Dirac Fermions in Graphene, *Phys. Rev. Lett.* **108**, 167401 (2012).
- [14] S. Wu, L. Mao, A. M. Jones, W. Yao, C. Zhang, and X. Xu, Quantum-enhanced tunable second-order optical nonlinearity in bilayer graphene, *Nano Lett.* **12**, 2032 (2012).
- [15] C. B. Mendl, M. Polini, and A. Lucas, Coherent terahertz radiation from a nonlinear oscillator of viscous electrons, *Appl. Phys. Lett.* **118**, 013105 (2021).
- [16] D. A. Bandurin, D. Svintsov, I. Gayduchenko, S. G. Xu, A. Principi, M. Moskotin, I. Tretyakov, D. Yagodkin, S. Zhukov, T. Taniguchi, K. Watanabe, I. V. Grigorieva, M. Polini, G. N. Goltsman, A. K. Geim, and G. Fedorov, Resonant terahertz detection using graphene plasmons, *Nat. Commun.* **9**, 5392 (2018).
- [17] M. Tokman, Y. Wang, I. Oladyshkin, A. R. Kutayiah, and A. Belyanin, Laser-driven parametric instability and generation of entangled photon-plasmon states in graphene, *Phys. Rev. B* **93**, 235422 (2016).
- [18] S. A. Mikhailov, Nonperturbative quasiclassical theory of graphene photoconductivity, *Phys. Rev. B* **103**, 245406 (2021).
- [19] S. A. Mikhailov, Theory of the strongly nonlinear electrodynamic response of graphene: a hot electron model, *Phys. Rev. B* **100**, 115416 (2019).
- [20] J. Cheng, N. Vermeulen, and J. Sipe, Second order optical nonlinearity of graphene due to electric quadrupole and magnetic dipole effects, *Sci. Rep.* **7**, 43843 (2017).
- [21] J. J. Dean and H. M. van Driel, Second harmonic generation from graphene and graphitic films, *Appl. Phys. Lett.* **95**, 261910 (2009).
- [22] J. J. Dean and H. M. van Driel, Second harmonic generation from graphene and graphitic films, *Phys. Rev. B* **82**, 125411 (2010).
- [23] M. Tokman, S. B. Bodrov, Yu. A. Sergeev, A. I. Korytin, I. Oladyshkin, Y. Wang, A. Belyanin, and A. N. Stepanov, Second harmonic generation in graphene dressed by a strong terahertz field, *Phys. Rev. B* **99**, 155411 (2019).
- [24] Y. Wang, M. Tokman, and A. Belyanin, Second-order nonlinear optical response of graphene, *Phys. Rev. B* **94**, 195442 (2016).
- [25] I. D. Tokman, Q. Chen, I. A. Shereshevsky, V. I. Pozdnyakova, I. Oladyshkin, M. Tokman, and A. Belyanin, Inverse faraday

- effect in graphene and weyl semimetals, *Phys. Rev. B* **101**, 174429 (2020).
- [26] M. Kim, S. G. Xu, A. I. Berdyugin *et al.*, Control of electron-electron interaction in graphene by proximity screening, *Nat. Commun.* **11**, 2339 (2020).
- [27] S. Tani, F. Blanchard, and K. Tanaka, Ultrafast Carrier Dynamics in Graphene under a High Electric Field, *Phys. Rev. Lett.* **109**, 166603 (2012).
- [28] K. J. Tielrooij, J. C. W. Song, S. A. Jensen, A. Centeno, A. Pesquera, A. Zurutuza Elorza, M. Bonn, L. S. Levitov, and F. H. L. Koppens, Photoexcitation cascade and multiple hot-carrier generation in graphene, *Nat. Phys.* **9**, 248 (2013).
- [29] M. Mittendorff, T. Winzer, E. Malic, A. Knorr, C. Berger, W. A. de Heer, H. Schneider, M. Helm, and S. Winnerl, Anisotropy of excitation and relaxation of photogenerated charge carriers in graphene, *Nano Lett.* **14**, 1504 (2014).
- [30] D. Brida, A. Tomadin, C. Manzoni, Y. J. Kim, A. Lombardo, S. Milana, R. R. Nair, K. S. Novoselov, A. C. Ferrari, G. Cerullo, and M. Polini, Ultrafast collinear scattering and carrier multiplication in graphene, *Nat. Commun.* **4**, 1987 (2013).
- [31] T. Ploetzing, T. Winzer, E. Malic, D. Neumaier, A. Knorr, and H. Kurz, Experimental verification of carrier multiplication in graphene, *Nano Lett.* **14**, 5371 (2014).
- [32] T. Winzer, E. Malic, and A. Knorr, Microscopic mechanism for transient population inversion and optical gain in graphene, *Phys. Rev. B* **87**, 165413 (2013).
- [33] T. Winzer, A. Knorr, and E. Malic, Carrier multiplication in graphene, *Nano Lett.* **10**, 4839 (2010).
- [34] E. Malic, T. Winzer, E. Bobkin, and A. Knorr, Microscopic theory of absorption and ultrafast many-particle kinetics in graphene, *Phys. Rev. B* **84**, 205406 (2011).
- [35] E. Malic, T. Winzer, and A. Knorr, Efficient orientational carrier relaxation in optically excited graphene, *Appl. Phys. Lett.* **101**, 213110 (2012).
- [36] G. Kane, M. Lazzeriand, and F. Mauri, High-field transport in graphene: the impact of zener tunneling, *J. Phys.: Condens. Matter.* **27**, 164205 (2015).
- [37] I. V. Oladyshkin, S. B. Bodrov, Y. A. Sergeev, A. I. Korytin, M. D. Tokman, and A. N. Stepanov, Optical emission of graphene and electron-hole pair production induced by a strong terahertz field, *Phys. Rev. B* **96**, 155401 (2017).
- [38] M. S. Foster and I. L. Aleiner, Slow imbalance relaxation and thermoelectric transport in graphene, *Phys. Rev. B* **79**, 085415 (2009).
- [39] J. C. W. Song, K. J. Tielrooij, F. H. L. Koppens, and L. S. Levitov, Photoexcited carrier dynamics and impact-excitation cascade in graphene, *Phys. Rev. B* **87**, 155429 (2013).
- [40] V. N. Kotov, B. Uchoa, V. M. Pereira, F. Guinea, and A. H. Castro Neto, Electron-electron interactions in graphene: Current status and perspectives, *Rev. Mod. Phys.* **84**, 1067 (2012).
- [41] C. H. Lui, K. F. Mak, J. Shan, and T. F. Heinz, Ultrafast Photoluminescence from Graphene, *Phys. Rev. Lett.* **105**, 127404 (2010).
- [42] H. Wang, J. H. Strait, P. A. George, S. Shivaraman, V. B. Shields, M. Chandrashekar, J. Hwang, F. Rana, M. G. Spencer, C. S. Ruiz-Vargas, and J. Park, Ultrafast relaxation dynamics of hot optical phonons in graphene, *Appl. Phys. Lett.* **96**, 081917 (2010).
- [43] C. Z. Cheng and G. Knorr, The integration of the Vlasov equation in configuration space, *J. Comput. Phys.* **22**, 330 (1976).
- [44] F. Filbet, E. Sonnendrücker, and P. Bertrand, Conservative numerical schemes for the Vlasov equation, *J. Comput. Phys.* **172**, 166 (2001).
- [45] <https://github.com/korzhimanov/Vasilek.jl>.
- [46] S. Bodrov, A. Murzanev, A. Korytin, and A. Stepanov, Terahertz-field-induced optical luminescence from graphene for imaging and near-field visualization of a terahertz field, *Opt. Lett.* **46**, 5946 (2021).
- [47] P. R. Whelan, Q. Shen, B. Zhou *et al.*, Fermi velocity renormalization in graphene probed by terahertz time-domain spectroscopy, *2D Mater.* **7**, 035009 (2020).